Experimental and Numerical Investigations of an Ice-slurry Generator

HONG Ruo-yu(洪若瑜)[1], DONG Liang(董梁)[2], SHANG De-yi(尚德义)[2]
XU Jian-sheng(徐建生)[2], Kawaji M[2]

(*1. Dept. Chem. & Chem. Eng., Soochow University, Suzhou, Jiangsu 215006, China;*
2. Dept. Chem. Eng. & Appl. Chem., University of Toronto, Toronto ON M5S 3E5, Canada)

Abstract：A new test facility equipped with refrigerant and brine circulation systems, and a rotating-scraper ice-slurry generator was constructed to analyze the ice-slurry flow and heat transfer accompanied by phase change in an industrial generator. The axial and transverse brine temperature and ice fraction concentration profiles in the ice generator were measured. The heat transfer efficiency lower than the average was identified in the upper half of the ice generator and its cause was determined by conducting three-dimensional numerical simulation using a commercial CFD code, FLUENT. Approaches of improving the brine-side heat transfer rates were investigated by incorporating extra mixing blades from numerical simulation.

Key words：ice generator; ice-slurry; numerical simulation; heat transfer
CLC No.：TQ022; TQ018 **Document Code**：A **Article ID**：1009–606X(2004)01–0001–07

1 INTRODUCTION

The application of ice-slurry production in fishery, poultry and food processing industries has a long history. A new emerging application is the ice generation, storage and processing for thermal storage. All the above applications involve the generation of ice. Optimal design and operation of ice generators are important for enhancing energy efficiency, increasing ice-slurry production capacity, and reducing the cost of ice-slurry production.

In some applications, space limitation and power requirements may make the use of ordinary ice generators unfeasible. The rotating-scraper ice-slurry generator is much smaller than the ordinary ones. Analyzing the multiphase flow and heat transfer in rotating-scraper ice-slurry generators would reduce the investment and operating costs.

Optimization of existing industrial apparatus requires knowledge of thermal-hydraulic characteristics inside ice-slurry generators, such as the rate of heat transfer with phase change and pressure drops with various ice fractions. Although some investigations have been carried out in the past on pressure drop and ice-slurry flow characteristics[1–3], and the heat transfer characteristics by melting ice[2,3], the characteristics of ice-slurry flow and heat transfer in industrial ice-slurry generators are still poorly understood.

Many companies and universities are doing related research and development, but only a few reports have been published[4–6]. Gosman et al.[4] proposed a numerical algorithm (PISO-2P) and

Received date: 2003–03–25, **Accepted date:** 2003–09–29
Foundation item: Supported by Key Lab. of Multiphase Reaction, IPE, CAS
Biography: HONG Ruo-yu(1966–), male, native of Suzhou city, Jiangsu Province, Ph. D., Professor, chemical engineering.

developed an in-house CFD code. The turbulent flows in stirred vessels were simulated using the code in that investigation. Fokema et al.[7] simulated fluid flow with strong rotation using a commercial code named FLOW3D. The computed results were compared with experimental measurements. Xu et al.[8] used the same CFD code to predict stirred tank flows, and the numerical data were compared with LDA measurements. Similar numerical simulations were conducted by Ranade et al.[9–11], Bakker et al.[12] using FLUENT code, and Djebbar et al.[13] using FIDAP code.

Recently, Sun et al.[14] conducted the 3-D numerical simulation of a stirred tank with an ASM (algebraic stress model) turbulence model. The model was embodied in their 3-D source code, and the numerical results were verified by literature data.

A new research facility was set up at Sunwell Technologies Inc., consisting of refrigerant (Freon R404A) and brine flow loops, and a rotating-scraper ice-slurry generator. The new facility was used to obtain heat transfer data in chilling and ice making modes. The brine-side flow and heat transfer characteristics were investigated both experimentally and numerically, and an inlet header was developed to distribute the refrigerant flow uniformly into the parallel cooling channels. This paper is concerned only with the brine-side behavior.

Fig.1 Outlook of the ice-slurry generator

2 EXPERIMENTAL

2.1 Test Loop

The outlook of ice-slurry experimental facility constructed at Sunwell Technologies Inc. is shown in Fig.1. The refrigeration capacity of the system is 19 kW, nominal production capacity (3.5% NaCl concentration, and 0°C makeup water temperature) is about 5 t/d. Freon R404A is used as the refrigerant.

2.2 Dimensions and Operating Conditions

The dimensions of the ice-slurry generator are listed in Table 1. The length of the brine flow channel was 1.6 m, with an I.D. of 15 cm. The radius of the hollow rotating shaft was 1.9 cm and the angel between wall and scraper was set at 60 degrees. The operating conditions of the ice-slurry generator are given in Table 2. At the inlet of brine, the temperature was 8°C (during the chilling mode) and the nominal velocity was 0.021 m/s (based on 15 cm I.D.). The shaft/scraper rotating speed was set at 0, 3, 6, or 10 r/s, respectively. The refrigerant temperature was assumed to be constant everywhere at –9°C and the heat transfer coefficient on the refrigerant side is about 7900 W/(m^2·K), which was calculated and provided by the Sunwell Technologies Inc.

Table 1 Dimensions of the ice-slurry generator

Length (m)	1.6	Length of outlet tube (cm)	10
Inner diameter (cm)	15	Angle between wall and blade (°)	60
Shaft radius (cm)	1.9	Wall thickness (between Freon and Brine) (mm)	3
Outlet tube radius (cm)	1.8		

Table 2 Typical operating conditions of the ice-slurry generator

Brine inlet temperature (°C)	8 (= –281.15 K)	Freon average temperature (°C)	–9 (=264.15 K)
Brine inlet velocity (m/s)	0.332 (=6 g/min)	Rotating speed of scraper (r/s)	6 (=360 r/min)

2.3 Experimental Procedure and Conditions

Experiments were performed during both the chilling and ice-making modes at different brine mass flow rates and cooling loads. Ice-slurry generation under different conditions was conducted using the test section. Typical flow conditions for the ice-slurry experiments are shown in Table 2.

2.4 Brine-side Temperature Measurements

In the present design, the ice scrapers inside the tubular ice generators are attached to a rotating shaft. The scrapers not only scratch ice crystals off the inner wall of the generator, but also enhance convection heat transfer by mixing the brine. In order to better understand the mixing effect, temperature distribution was measured inside the brine flow channel using thermistor arrays shown in Fig.2. The scraper-rotating shaft assembly was equipped with 25 fast-response (~1 s in water) and high-accuracy (±0.1°C in flowing water) thermistors to measure the brine temperature at five axial positions (A to E corresponding to 0.61, 0.91, 1.35, 1.83, and 2.23 m from the top) and four or five radial positions between the shaft and wall at each elevation. The transmission of 25 thermistor signals from a rotating shaft to a data acquisition system required the use of an infrared transmitter.

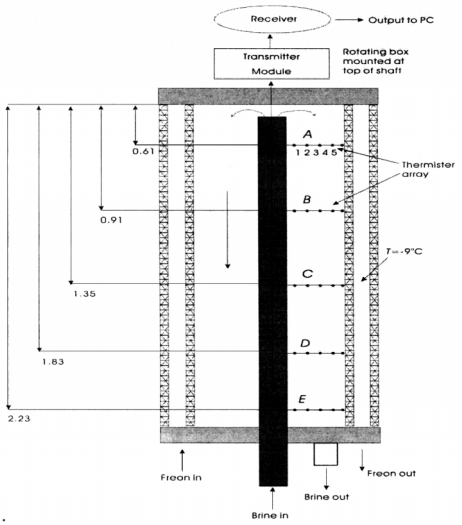

Fig.2 Sketch showing the structure of ice-slurry generator

The brine temperatures obtained during the chilling mode of operation are shown in Fig.3. At each axial position, little variation is observed in the radial temperature distribution from the four radial positions. Thus the fifth one was added, which is only 1 mm away from the wall. When the refrigerant flow was stopped during the test between about 210 and 500 s, all the temperatures converged to the same value. An isothermal condition was reached inside the ice-slurry generator. With the refrigerant flowing and cooling the brine, the axial temperature profiles obtained indicated lower heat transfer rates in the upper section compared to the lower section of the ice generator. Such lower heat transfer phenomena are not clear and more measurements are needed to determine its cause. The overall heat transfer rate may be further improved by modifying the scraper design and enhancing the radial velocity component and mixing of the brine.

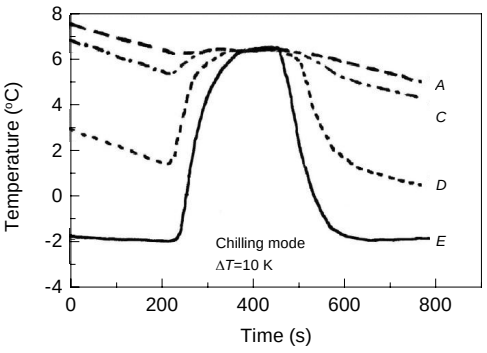

Fig.3 Brine temperature distribution during a chilling mode at a typical condition shown in Table 2

3 NUMERICAL SIMULATION

3.1 Governing Equations

The governing equations describing fluid flow in ice generator were listed in Table 3. The

mixture is assumed as incompressible Newtonian fluid since the ice concentration is relatively low. Thus the viscous stress tensor can be found easily in reference[4,14].

Table 3 Governing equations

Continuity equation:	$\mathrm{div}(\rho\vec{U}) = 0,$	(1)
U momentum equation:	$\mathrm{div}(\rho\vec{U}U) = -\frac{\partial p}{\partial z} + \mathrm{div}\,\tau_x + F_x,$	(2)
V momentum equation:	$\mathrm{div}(\rho\vec{U}V) - \rho\frac{W^2}{r} = -\frac{\partial p}{\partial r} + \mathrm{div}\,\tau_v - \frac{\tau_{r\theta}}{r} + F_v,$	(3)
W momentum equation:	$\mathrm{div}(\rho\vec{U}W) + \rho\frac{VW}{r} = -\frac{1}{r}\frac{\partial p}{\partial \theta} + \mathrm{div}\,\tau_\theta + \frac{\tau_{r\theta}}{r} + F_\theta,$	(4)
k equation:	$\mathrm{div}(\rho\vec{U}k) = \mathrm{div}\left(\frac{\mu}{\alpha_k}\mathrm{grad}k\right) + (G_k - \rho\varepsilon),$	(5)
ε equation:	$\mathrm{div}(\rho\vec{U}\varepsilon) = \mathrm{div}\left(\frac{\mu}{\alpha_\varepsilon}\mathrm{grad}\varepsilon\right) + \frac{\varepsilon}{k}(C_1G_k - C_2\rho g\varepsilon).$	(6)

Note: The body forces, F_x, F_r and F_θ, include gravity, centrifugal and Coriolis terms, which arise only when a rotating reference frame is used. $F_x = -\rho g$, $F_r = \rho(\omega^2 r + 2\omega W)$, $F_\theta = \rho(-2\rho V)$.

3.2 Solution Procedure

In order to further analyze the brine temperature distribution measured in the tubular ice-slurry generator as described above and to explore ways of improving the heat transfer rates, numerical modeling and simulation of the brine flow in the tubular ice generator was conducted using a commercial CFD code, FLUENT version 5.3, which is based on control volume approach. The simulation involved modeling 3-D incompressible turbulent flow with strong rotation in complex geometry. A steady flow was assumed in a rotating frame of reference, and a standard k–ε turbulence model was used for turbulence modeling. Other turbulence models were also tried, it was found that the current model was the most stable and gave satisfactory results.

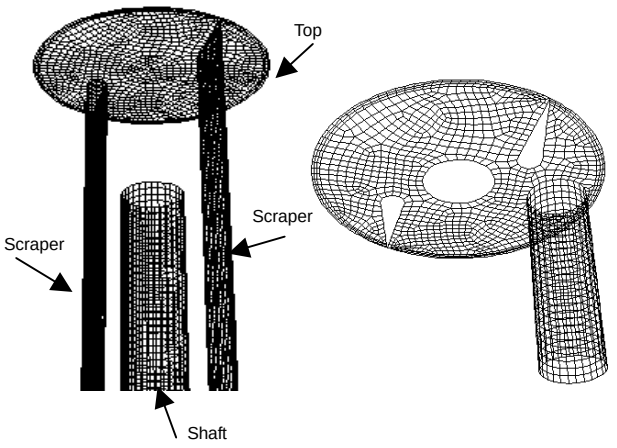

(a) Mesh showing top, inlet tube and scrapers of the ice-slurry (b) Mesh showing bottom and outlet tube of the ice-slurry generator

Fig.4 Surface meshes

3.3 Computational Mesh

The Gambit (version 1.3, Fluent Inc.) software was used to create unstructured grids of hexahedral mesh elements. Figure 4(a) shows the surface meshes at the top of the ice generator, with two rotating-scraper blades attached to a rotating shaft at the center. Figure 4(b) shows the surface mesh at the bottom of the ice-slurry generator and the outlet tube.

4 RESULTS AND DISCUSSION

4.1 Experimental Measurement vs. Numerical Results

All the cases modeled in this investigation were in the chilling mode. The physical properties

of water and ice at 0°C were used in the numerical computations.

Figure 5 shows a comparison of numerical predictions (solid line) with a measured axial temperature profile (dashed line). The axial temperature variation was predicted reasonably well in the lower section, and some difference was observed between the upper and lower sections of the ice generator.

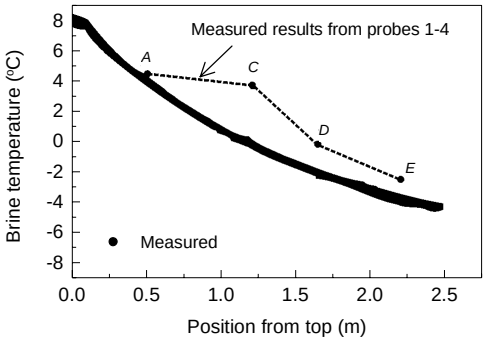

Fig.5 Comparison of predicted and measured axial temp. profiles at a typical condition shown in Table 2

4.2 Influence of Rotation Speed

The computed axial temperature profiles at 0 and 3 r/s were shown in Fig.6(a) and Fig.6(b), respectively. The effect of rotating speed on the exit brine temperature was significant at low rotation speeds (<3 r/s), but became reduced at higher rotation speeds. At a rotation speed of 6 r/s, the exit brine temperature was about 1.5 K lower than that at a rotation speed of 3 r/s.

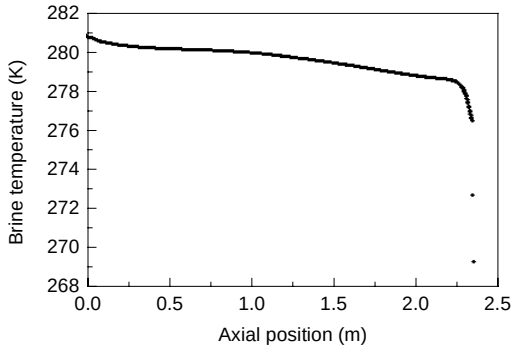

(a) Axial temperature profile along line 1 at 0 r/m

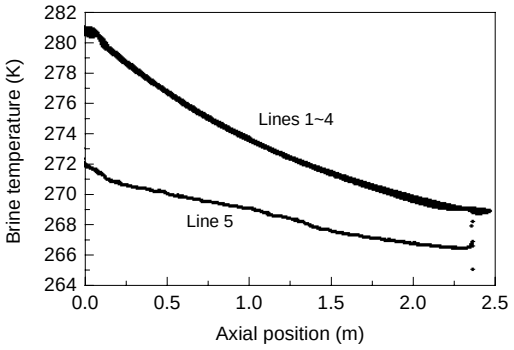

(b) Axial temperature profiles along line 1~5 at 3 r/m

Fig.6 Axial temperature profiles at 0 and 3 r/s [other conditions are shown in Table 2, lines 1~5 are vertically passing through points 1~5 in Fig.7(b)]

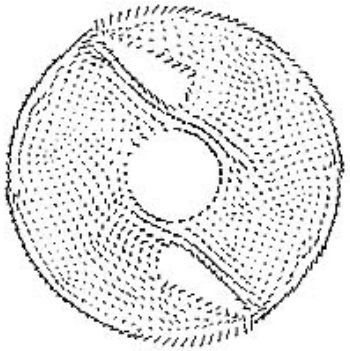

(a) Overall velocity vectors in a cross-section

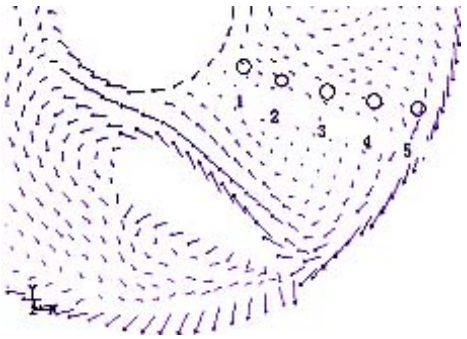

(b) Local velocity vectors in a cross-section

Fig.7 Velocity vectors in a cross-section area (at a typical condition shown in Table 2)

At a rotating speed of 6 r/s, the computed velocity vectors of a cross-section area in the middle of the ice-slurry generator are shown in Fig.7(a) and 7(b). The former shows the overall velocity vector in the cross-section, while the later shows the velocity vector near the scraper. It can be seen that the flow pattern is very complicated in the rotating-scraper ice-slurry generator. The radial velocity is relatively high, and it will be difficult to improve the heat transfer rate by increasing the radial flow.

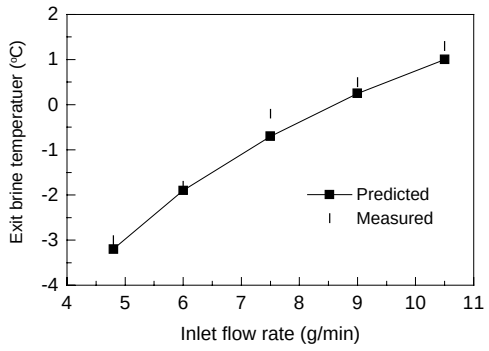

Fig.8 Computed and measured exit temperatures at different flow rates (other conditions are shown in Table 2)

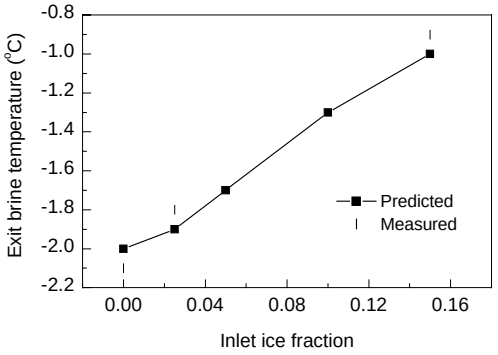

Fig.9 Exit brine temperature vs. inlet ice concentration (other conditions are shown in Table 2)

4.3 Influence of Extra Scraper

To further improve heat transfer in the upper as well as the lower sections, extra mixing blades/scrapers near the shaft were added to the model to induce greater radial velocities in the brine flow field. A case with three scraper blades was also examined numerically for a rotation speed of 180 r/min(=3 r/s). The results showed greater heat transfer rates, but further work is necessary to determine the optimum blade geometry and arrangement. The effect of rotating speed on the exit brine temperature was significant at low rotation speeds (<3 r/s), but became reduced at higher rotation speeds. At a rotation speed of 6 r/s, the exit brine temperature was lower by 0.5 K if extra blades were used.

4.4 Exit Brine Temperature vs. Inlet Flow Rate

Figure 8 shows the influence of inlet flow rate on exit brine temperature. The heat exchange rate increases with the increasing inlet flow rate. But the exit brine temperature increases as well. When the inlet flow rate is 6 g/min (=0.0227 m^3/min), the exit brine temperature is about –2.1°C, which was verified by experimental results. Further increase of the inlet flow rate will result in a decrease of ice productivity. Thus the inlet brine flow rate should be lower than 6 g/min.

4.5 Exit Brine Temperature vs. Inlet Ice Fraction

The viscosity of ice-slurry is influenced by ice fraction. Recently, the Danish Technological Institute that worked closely with the authors provided a better estimate to calculate the mixture viscosity: $\mu=\mu_b(1+4.5c_{ice})$. Figure 9 shows the influence of inlet ice fraction on exit brine temperature. When the ice is excessive in slurry, the mixture viscosity will be too high, which will result in a low heat transfer between the ice-slurry and the cylinder wall. The predicted result was verified by experiments.

5 CONCLUSIONS

A new ice-slurry research facility with 150 cm I.D. has been developed that enables the investigation of ice-slurry flow and heat transfer characteristics in a rotating-scraper ice-slurry generator. The brine and refrigerant side flow loops have been completed and the ice-slurry generator test section was constructed with instrumentation for measuring brine temperature. Commissioning tests were conducted to collect temperature and heat transfer data. Axial and radial temperature distributions were measured and numerically predicted. An apparently lower heat transfer rate from measurements was found in the upper section of the ice generator compared to that in the lower section. The radial velocity around the scrapers was relatively high. An improved design with three scrapers was recommended to improve the heat transfer rate in the entire ice generator.

NOTATIONS:

c_{ice}	Ice fraction	r	Radial direction (m)	μ_b	Brine viscosity (N·s/m^2)
$\vec{g}$	Gravity vector (m/s^2)	t	Time (s)	ρ	Fluid average density (kg/m^3)
k	Turbulent kinetic energy (m^2/s^2)	$\vec{U}$	Velocity vector, =(U,V,W) (m/s)	ω	Angular velocity (r/s)
p	Fluid pressure (Pa)	x,y,z	Spatial directions (m)	τ	Viscous stress tensor (N/m^2)
Pe	Grid Peclet number	Δt	Time step (s)	θ	Azimuthal direction (m)
R	Radius of the cylinder (m)	μ	Fluid average viscosity (N·s/m^2)		

REFERENCES:

[1] Gupta R P, Fraser C A. Effect of a New Friction Reducing Additive on Sunwell Ice Slurry Characteristics [R]. Report No. TR–LT–023, NRC, No.32123. National Research Council of Canada, Institute of Mechanical Engineering, Low Temperature Laboratory, 1990.

[2] Bellas J, Chaer I, Tassou S A. Heat Transfer and Pressure Drop of Ice Slurries in Plate Heat Exchangers [J]. Appl. Therm. Eng., 2002, 22(7): 721–732.

[3] Knodel B D, France D M, Choi U S, et al. Heat Transfer and Pressure Drop in Ice-water Slurries [J]. Appl. Therm. Eng., 2000, 20(7): 671–685.

[4] Gosman A D, Lekakou C, Politis S, et al. Multidimensional Modeling of Turbulent Two-phase Flows in Stirred Vessels [J]. AIChE. J., 1992, 38(12): 1946–1956.

[5] Kitanovski A, Poredos A. Concentration Distribution and Viscosity of Ice-slurry in Heterogeneous Flow [J]. Int. J. Refriger., 2002, 25: 827–835.

[6] Ismail K A R, Radwan M M. Modeling of Ice Crystal Growth in Laminar Falling Films for the Production of Pumpable Ice Slurries [J]. Energ. Convers. Manage., 2002, 44: 65–84.

[7] Fokema M D, Kresta S M, Wood P E. Importance of Using the Correct Impeller Boundary Conditions for CFD Simulations of Stirred Tanks [J]. Can. J. Chem. Eng., 1994, 72: 177–183.

[8] Xu Y, McGrath G. CFD Predictions of Stirred Tank Flows [J]. Trans. IChemE., 1996, 74(Part A): 471–475.

[9] Ranade V V, Dommeti S M S. Computational Snapshot of Flow Generated by Axial Impellers in Baffled Stirred Vessels [J]. Trans. IChemE., 1996, 74(Part A): 476–484.

[10] Tanguy P A, Bertrand F, Labrie R, et al. Numerical Modeling of the Mixing of Viscoplistic Slurries in a Twin-blade Planetary Mixer [J]. Trans. IChemE., 1996, 74(Part A): 499–503.

[11] Morud K E, Hjertager B H. LDA Measurements and CFD Modeling of Gas–Liquid Flow in a Stirred Vessel [J]. Chem. Eng. Sci., 1996, 51(2): 233–249.

[12] Bakker A, Myers K J, Ward R W, et al. The Laminar and Turbulent Flow Pattern of a Pitched Blade Turbine [J]. Trans. IChemE., 1996, 74(Part A): 485–491.

[13] Djebbar R, Roustan M, Line A. Numerical Computation of Turbulent Gas–Liquid Dispersion in Mechanical Agitated Vessels [J]. Trans. IChemE., 1996, 74(Part A): 492–498.

[14] Sun H Y, Wang W J, Mao Z S. Numerical Simulation of the Whole Three-dimensional Flow in a Stirred Tank with Anisotropic Algebraic Stress Model [J]. Chinese J. Chem. Eng., 2002, 10(1): 15–24.